Fechner, D.; Blawert, C.; Hort, N.; Dieringa, H.; Kainer, K.U. **:**

Development of a magnesium secondary alloy system for mixed magnesium post-consumer scrap

In: Materials Science and Engineering A (2013) Elsevier

DOI: 10.1016/j.msea.2013.03.053

Development of a Magnesium Secondary Alloy System for Mixed Magnesium Post-Consumer Scrap

Daniel Fechner[a,1], Carsten Blawert[a], Norbert Hort[a], Hajo Dieringa[a], Karl Ulrich Kainer[a]

[a] Magnesium Innovation Centre MagIC, Institute of Materials Research, Helmholtz-Zentrum Geesthacht, Max-Planck-Straße 1, 21502 Geesthacht, Germany

[1] corresponding author, present affiliation:
TÜV NORD Systems GmbH & Co. KG,
Competence Centre Materials and Welding Technology, Technikzentrum,
Große Bahnstaße 31, 22525 Hamburg, Germany
e-mail: dfechner@tuev-nord.de
Phone: +49 40 8557-1097, Fax: +49 40 8557-2710

Abstract

Six alloys were prepared by high pressure die casting in order to develop a magnesium secondary alloy system for mixed post-consumer scrap. The alloys were investigated with regard to intermetallic phases, grain structures, mechanical properties and performance in the salt spray test. The results are discussed in relation to the characteristics of the high pressure die casting process. The effect of contamination by copper and compensation for this effect by the addition of zinc

were thoroughly investigated for the most promising alloy. It is evident that the alloying elements strontium, silicon and calcium are incorporated in the ternary Zintl phase $Sr_{6.33}Mg_{16.67}Si_{13}$, while aluminium, zinc, copper and magnesium form the tau-phases $Mg_{32}(Al_x,Cu_{1-x})_{49}$ and $Mg_{32}(Al,Zn)_{49}$. The two tau-phases can merge due to isomorphism. $Mg_{32}(Al,Zn)_{49}$ ensures improved corrosion resistance after the addition of copper.

Keywords: magnesium alloys, secondary alloy, corrosion, mechanical characterization, intermetallics, HPDC

1 Introduction

The primary production of magnesium has increased considerably over the last 15 years [1-3]. Approximately half of world output is used for alloy production, and the alloys are predominantly used in the automotive sector. The present trend to reduce CO_2 emissions of vehicles driven by internal combustion engines might support an increasing use of magnesium alloys in the future. In the case of electric vehicles and fuel cell vehicles, enhanced driving range could be achieved if magnesium components were used in their construction. Increasing use of magnesium for automotive components and larger volumes of magnesium scrap from end-of-life vehicles (ELVs) are therefore probable. Gesing [4] and Scharf [5] consider scrap from ELVs to be the greatest source of magnesium post-consumer scrap. The greater the quantity of scrap material, the more viable the recycling process becomes. The primary production of magnesium is very energy-intensive [6] and it has been shown that magnesium recycling can have a considerable impact on the overall energy- and CO_2-balance of automotive vehicles [7]. However, so far only clean magnesium scrap sorted according to one alloy composition is recycled by

means of re-melting. If magnesium scrap from automotive vehicles is to be reused, two problems must be considered. The shredder process is most commonly used today for processing ELVs, and for economic reasons it is also likely to be used in the future [8]. Shredding on the one hand causes intermixture of different magnesium alloys and their incorporated alloying elements, whilst on the other hand, it implies the contamination of magnesium with iron, nickel and copper. Iron is part of every scrap fraction. Nickel and copper are common alloying elements for aluminium or are even used as coatings for magnesium components. Iron, nickel and copper are most detrimental to the corrosion resistance of magnesium. The iron content in magnesium melts can be controlled by the addition of manganese, but the level of nickel and copper can only be influenced by distillation or dilution. Dilution is considered impracticable on an industrial scale [8]. Distillation consumes approximately 5-7.5 KWh/kg [6, 9].

The idea of secondary alloys is to re-melt scrap metal for the fabrication of new components whilst using a minimum of primary material to achieve the required composition. In the case of magnesium scrap, re-melting consumes at most half the energy that is needed for distillation [6]. Re-melting of post-consumer scrap is already carried out in the case of aluminium, and alloys such as AlSi9Cu3 and AlSi12Cu are established as suitable for recycling. However, special alloys have to be developed for magnesium due to its sensitivity towards the aforementioned impurities. According to Barannik [10], a secondary alloy for utilisation of magnesium scrap material was used in the former USSR. However, the alloy was used only for steel desulphurisation and as an alloying element in the aluminium industry.

There has been extended research on the development of secondary magnesium alloys by the TU-Clausthal and the Helmholtz Zentrum Geesthacht, formerly GKSS Research Centre Geesthacht [5, 11-13]. Two alloys - AZC1231 and AZC531 - have been patented [14, 15]. In alloy AZC1231, copper and nickel are incorporated into the so-called τ–phase $Mg_{32}(Al,Zn)_{49}$. Iron is incorporated into aluminium-manganese precipitates. Additionally, an increased aluminium content causes the formation of a continuous network of the $Mg_{17}Al_{12}$ phase. The network acts as a corrosion barrier and increases the corrosion resistance of the material. However, the increased content of intermetallic phases reduces the elongation at fracture. A second alloy with increased ductility was therefore developed. In alloy AZC531, the aluminium content is reduced to suppress the formation of the $Mg_{17}Al_{12}$ phase almost entirely. Both secondary alloys contain approximately 3 % zinc for the formation of the $Mg_{32}(Al,Zn)_{49}$ phase. The zinc concentration is a compromise between the corrosion resistance, the suppression of the $Mg_{17}Al_{12}$ phase, the ductility of the alloy and the cost of the primary materials [11]. Whilst an increase in tolerance limits for impurities has been successfully achieved, no research has been undertaken on the interaction of alloying elements from different commercial magnesium alloys. An improved understanding of the phase formation in complex alloy systems is essential for the development and use of secondary alloys of magnesium.

Most automotive magnesium components nowadays are fabricated from high pressure die casting alloys based on the magnesium-aluminium-zinc and the magnesium-aluminium-manganese systems, i.e. AZ and AM systems [16]. With the invention of several cost-competitive, heat-resistant alloys, the variety of magnesium materials for castings has been considerably broadened. This development has

allowed the fabrication of an increasing number of drive train components such as gearbox housings and crankcases [17, 18]. The most important of these materials are based on the AM system, with either strontium, silicon or calcium ensuring thermal stability. Common representatives of these alloys are AJ52A, AJ62A [19], AS31 [17], MRI153M and MRI230D [20, 21]. In alloy AXJ530, both calcium and strontium are used [21]. The aforementioned materials have two things in common with regard to their chemical compositions. They contain approximately 0.3 % manganese and between 1.8 and 8.4 wt% aluminium. The high pressure die casting alloy AM50 can therefore be regarded as their lowest common denominator.

The aim of this project was the development of a secondary alloy for mixed magnesium scrap from ELVs. Several alloys based on the alloy AM50 were prepared for this purpose. The chemical compositions were meant to represent those of potentially emerging magnesium scrap, containing different quantities of strontium, silicon and calcium. After previous work on permanent mould-cast materials [22-24], alloys with moderate contents of the three elements were chosen for further investigations. XRD analysis proved the formation of the ternary Zintl phase $Sr_{6.33}Mg_{16.67}Si_{13}$ when strontium, silicon and calcium were present [23]. The precipitate formed preferentially instead of the Al_4Sr, $Mg_{17}Sr_2$ and Mg_2Si phases. The formation of $Sr_{6.33}Mg_{16.67}Si_{13}$ and its effect on the mechanical properties has been recently described [25]. EDX measurements revealed that the intermetallic phase solves calcium [22] and it was supposed that strontium atoms were substituted for calcium atoms due to a similar atomic radius [25].

Six alloys were prepared by high pressure die casting (HPDC), the most common casting technique for automotive magnesium components. The base material AM50 was the first alloy. Strontium, silicon and calcium were subsequently added in order to prepare the second, third and fourth alloys. For the fifth alloy, the addition of impurities during the shredder process was simulated by the addition of 0.5% copper. For the sixth alloy, zinc was added in order to reduce the effect of the previous contamination and to restore the corrosion resistance. The phase formation as well as the mechanical properties and the performance in a salt spray test were investigated in detail for all alloys. The results of this study demonstrate how the problems of mixed alloying elements and of contamination with impurities can be addressed in one alloy system.

2 Experimental Methods

Six alloys were prepared by HPDC. A FRECH cold chamber machine with a locking force of 450 t was used for casting. Sectioned ingots of alloy AM50 were melted at 680 °C in the feeding furnace of the machine. The alloying elements were added in their pure form. The melt was stirred for 60 minutes and allowed to settle for 30 minutes before casting. A mixture of argon and 0.2 vol% SF_6 was used to prevent melt oxidation. The die temperature was set to 250 °C.

The chemical composition was determined using optical emission spectroscopy (OES). For XRD investigations, a diffractometer with a Cu anode was used. The acceleration voltage was adjusted to 40 kV and the cathode current to 30 mA. The step size was set to 0.05° and the step time to 8 s. Microstructural investigations and phase analysis were performed by optical microscopy, scanning electron microscopy

and X-ray diffraction. Grain sizes were determined using the linear intercept method according to ASTM standard E 112 – 96 [26]. The porosity was measured using the Archimedes principle. Tensile tests were performed according to DIN EN 10002-1 [27]. Flat tensile specimens were cut from 2 mm-thick HPDC plates by spark erosion cutting according to DIN 50125 [28]. Round, cylindrical specimens with a diameter of 6 mm and a length of 15 mm for compression creep tests were machined by turning. The creep tests were carried out for 200 h at 60 MPa and 150 °C. The minimum creep rates were calculated from the last ten hours of the tests. The salt spray tests were performed according to ASTM standard B 117 - 07 [29]. The corrosion specimens were ground with 1200-grit silicon carbide paper and cleaned in ethanol prior to testing. While “as cast” samples were ground only on the cutting edges, “ground” samples were finished on all surfaces. The tests were performed for 48 h using a 5 % NaCl solution at pH 7. All tests were repeated three times, and the average values and their standard deviations are presented.

3 Results

3.1 Chemical Analysis

Table 1 shows the chemical composition of the alloys and the specification of alloy AM50A according to ASTM standard B 94 – 07 [30]. Except for the two Cu-containing materials, the levels of impurities are within the thresholds specified by the standard.

Table 1: Chemical composition of HPDC alloys in wt%, Mg remainder

Alloys	Al	Mn	Sr	Si	Ca	Zn	Cu	Fe	Ni
AM50A[a]	4.4-5.4	0.26-0.6	-	0.10	-	0.22	0.010[b]	0.004[b]	0.002
AM50	4.74	0.27	0.00	0.02	0.00	0.01	0.0011	0.0015	0.0003
AJM50	4.75	0.32	0.45	0.02	0.00	0.01	0.0011	0.0030	0.0003
AJMS50	4.72	0.31	0.43	0.17	0.00	0.01	0.0012	0.0031	0.0003
AJMSX50	4.85	0.31	0.45	0.17	0.15	0.01	0.0013	0.0031	0.0003
ACJMSX50	4.73	0.28	0.49	0.17	0.13	0.01	0.45	0.0026	0.0003
AZCJMSX53	4.59	0.30	0.46	0.16	0.13	3.20	0.43	0.0031	0.0003
[a] ASTM B 94 – 07, [b] max									

3.2 Phase Formation & Microstructure

Fig. 1 shows the XRD patterns of the copper-free alloys including alloy AM50. The constituents of the base alloy are the α-matrix and the $Mg_{17}Al_{12}$ phase. The Al_4Sr phase was detected after the addition of strontium. The intensity of the strongest peak of the $Mg_{17}Al_{12}$ phase at 2θ of approximately 36° clearly decreased compared to alloy AM50. The ternary Zintl phase $Sr_{6.33}Mg_{16.67}Si_{13}$ formed after the addition of silicon. No other phases were detected after the addition of calcium, but the intensity of the Al_4Sr peaks is higher for alloy AJMSX50 than for alloy AJMS50. Fig. 2 shows the XRD patterns of the two copper-free alloys AM50 and AJMSX50 together with those of the alloys ACJMSX50 and AZCJMSX53. The $Mg_{17}Al_{12}$ and the Al_4Sr phase were not detectable after the addition of copper. Two peaks emerging in the XRD pattern of alloy ACJMSX50 at 2θ of approximately 38° and 39° could not be identified using the available database. However, the peaks are similar to those ascribed to the $Mg_{32}(Al,Zn)_{49}$ phase after the addition of zinc, i.e., in alloy AZCJMSX53. The ternary Zintl phase $Sr_{6.33}Mg_{16.67}Si_{13}$ is present in the alloys ACJMSX50 and AZCMSX53.

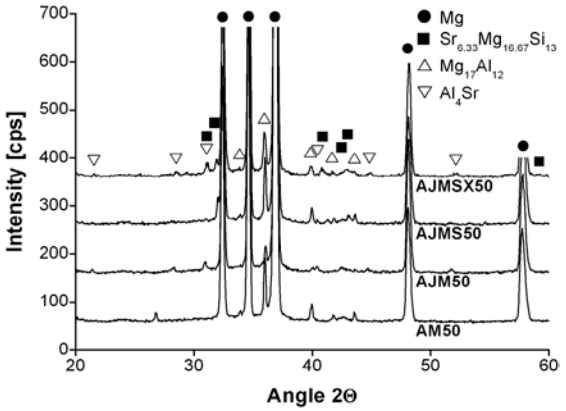

Fig. 1: XRD patterns of the Cu-free alloys

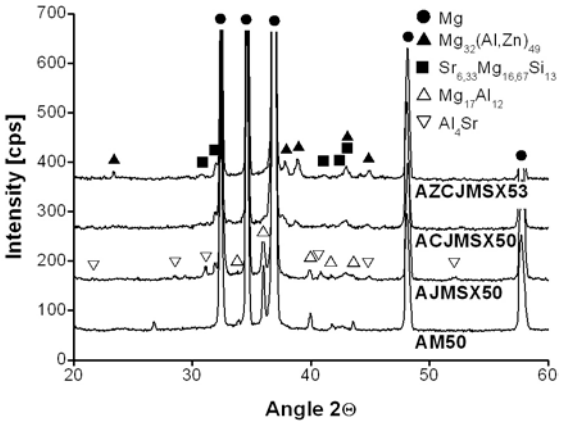

Fig. 2: XRD patterns of alloys AM50, AJMSX50, ACJMSX50 and AZCJMSX53

Fig. 3 and Fig. 4 show SEM images of the copper-containing alloy ACJMSX50. The phase compositions determined by EDX analysis are presented in Table 2. The α-matrix contains predominantly aluminium in solid solution. The Al-Sr precipitates have an Al/Sr ratio of 5.4 but an Al/(Sr+Ca) ratio of 3.7. The precipitates have a lamellar structure. For $Sr_{6.33}Mg_{16.67}Si_{13}$, a (Sr+Ca)/Mg/Si ratio of 3/9/6 is calculated. Considerable amounts of oxygen and carbon are measured. The Mg-Al-Cu phase incorporates elevated contents of strontium and calcium and exhibits a compact shape. Copper is predominantly found in the Mg-Al-Cu phase and the Al-Sr precipitates. The α–matrix, Al-Mn and $Sr_{6.33}Mg_{16.67}Si_{13}$ precipitates are nearly free of copper.

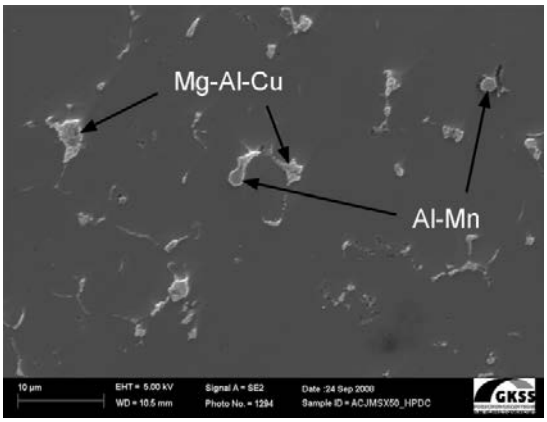

Fig. 3: Microstructure of alloy ACJMSX50, SEM

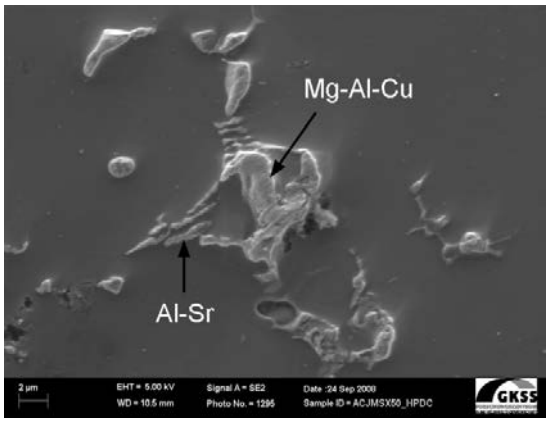

Fig. 4: Microstructure of alloy ACJMSX50, detail, SEM

Table 2: Phase analysis based on EDX measurements in alloy ACJMSX50

Elements	EDX analysis of intermetallic phases [At%]				
	α-Matrix [a]	Al-Mn	Al-Sr	Mg-Al-Cu	$Sr_{6.33}Mg_{16.67}Si_{13}$
Mg	97.4 ± 0.3	25.5 ± 21.0	14.3 ± 5.8	48.6 ± 6.1	40.6 ± 7.0
Al	2.2 ± 0.3	32.9 ± 8.7	57.6 ± 2.8	34.4 ± 5.3	1.8 ± 0.1
Mn	0.1 ± 0.0	26.4 ± 9.8	2.4 ± 0.4	[b]	[b]
Sr	[b]	0.2 ± 0.0	10.6 ± 1.3	1.4 ± 0.4	10.1 ± 2.0
Si	[b]	5.1 ± 1.3	0.1 ± 0.2	0.1 ± 0.1	26.6 ± 0.7
Ca	0.1 ± 0.0	0.1 ± 0.0	5.1 ± 1.3	2.7 ± 0.6	4.8 ± 1.3
Cu	0.1 ± 0.0	0.1 ± 0.1	4.5 ± 0.2	7.4 ± 1.7	0.2 ± 0.1
Zn	[b]	[b]	[b]	[b]	[b]
O	0.3 ± 0.0	9.9 ± 1.1	3.9 ± 1.2	2.3 ± 0.9	9.9 ± 8.3
C	[b]	[b]	3.9 ± 1.8	3.1 ± 0.7	6.1 ± 2.6
Voltage	15 kV	15 kV	5 kV	5 kV	5 kV

[a] measured in the casting skin of the 2 mm-thick HPDC plate, [b] unable to be measured

Fig. 5 and Fig. 6 show the microstructure of the zinc-containing alloy AZCJMSX53. The phase compositions determined by EDX analysis are presented in Table 3. In addition to aluminium, the α-matrix now contains zinc to a limited extent. Al-Sr precipitates are no longer detected. For $Sr_{6.33}Mg_{16.67}Si_{13}$ a (Sr+Ca)/Mg/Si ratio of 3/19/7 is calculated. The amount of oxygen and carbon is even higher than for alloy ACJMSX50. $Mg_{32}(Al,Zn)_{49}$ is rich in aluminium, zinc and copper and exhibits large variations in the chemical composition. Additionally, the phase contains strontium and calcium. Al-Mn precipitates contain a limited amount of copper. No copper was detected in the α–matrix or the $Sr_{6.33}Mg_{16.67}Si_{13}$ phase.

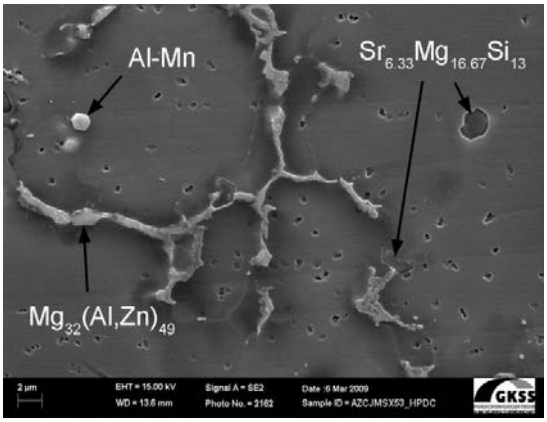

Fig. 5: Microstructure of alloy AZCJMSX53, SEM

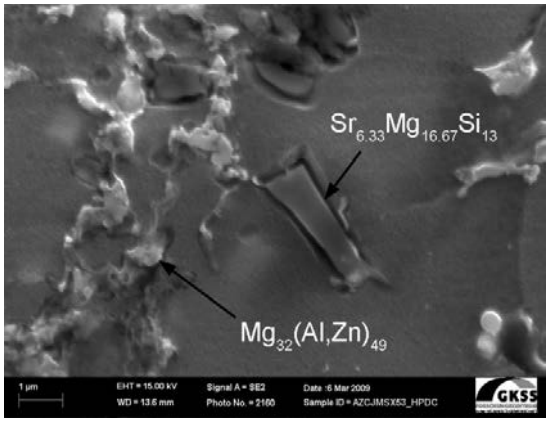

Fig. 6: Microstructure of alloy AZCJMSX53, detail, SEM

Table 3: Phase analysis based on EDX measurements in alloy AZCJMSX53

Elements	EDX analysis of intermetallic phases [At%]			
	α-Matrix [a]	Al-Mn	$Mg_{32}(Al,Zn)_{49}$	$Sr_{6.33}Mg_{16.67}Si_{13}$
Mg	95.9 ± 1.0	11.2 ± 14.0	67.3 ± 15.8	50.1 ± 10.6
Al	3.0 ± 0.7	46.5 ± 11.6	18.9 ± 8.0	2.4 ± 1.1
Mn	[b]	37.6 ± 3.4	[b]	[b]
Sr	[b]	1.4 ± 0.8	0.6 ± 0.0	5.2 ± 1.7
Si	[b]	3.3 ± 2.1	[b]	18.7 ± 5.0
Ca	[b]	[b]	0.6 ± 0.3	2.9 ± 0.9
Cu	[b]	0.2 ± 0.2	2.4 ± 1.9	[b]
Zn	0.6 ± 0.2	0.4 ± 0.1	9.8 ± 5.7	0.5 ± 0.2
O	0.3 ± 0.0	1.5 ± 1.7	0.4 ± 0.2	12.9 ± 3.6
C	[b]	1.8 ± 1.0	[b]	7.2 ± 0.7
Voltage	15 kV	15 kV	15 kV	15 kV
[a] measured in the casting skin of the 2 mm thick HPDC plate, [b] unable to be measured				

3.3 Mechanical Properties in the Tensile Test

Fig. 7 shows the tensile yield strength of all the alloys plotted together with the inverse square root of the grain diameter. It has to be noted that due to the so-called “skin effect” the microstructure of high pressure die cast magnesium alloys shows a bimodal grain size distribution. The values are therefore given for grains of the casting skin, s, and grains near the centre of the casting, c. It can be seen that the inverse square root of the two grain diameters correlates with the development of the tensile yield strength.

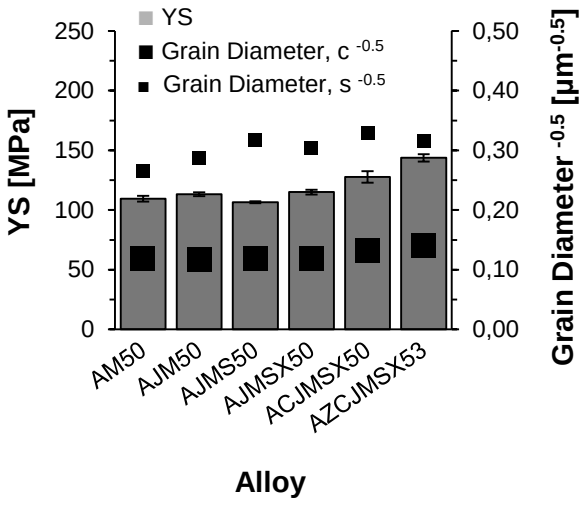

Fig. 7: Yield strength and inverse square root of the grain diameter – c-centre, s-casting skin

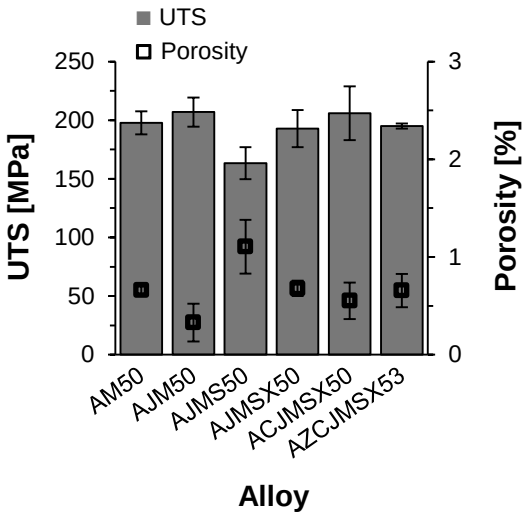

Fig. 8: Ultimate tensile strength and porosity

In Fig. 8 and Fig. 9, the ultimate tensile strength and the elongation at fracture for all six alloys are presented, together with the porosity of the tested samples. Clear contrary behaviour can be seen between the two mechanical parameters and the number of pores. Independently of the porosity, the elongation at fracture decreases as the amount of alloying elements increases. This effect is most obvious when comparing the base alloy AM50 to the Zn-containing alloy AZCJMSX53. The samples exhibit approximately the same level of porosity.

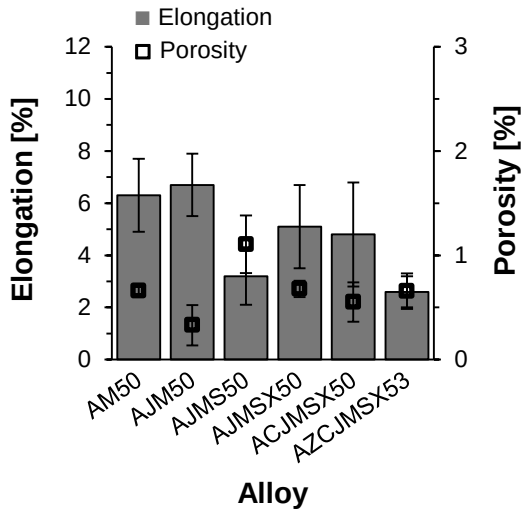

Fig. 9: Elongation at fracture and porosity

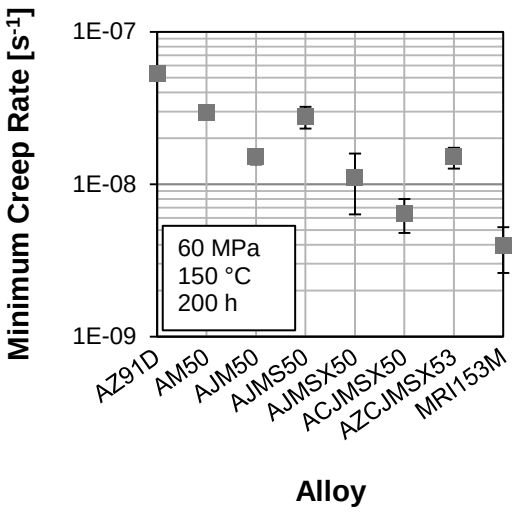

Fig. 10: Minimum creep rate, compression creep, 60 MPa, 150 °C, 200 h

3.4 Compression Creep Tests

Fig. 10 shows the minimum creep rates of the six alloys. The commercial alloys AZ91D and MRI153M are included for comparison. The addition of strontium reduces the creep rate compared to the base material AM50. After the subsequent addition of silicon, the creep rate exceeds the level of alloy AJM50. The addition of 0.2 % calcium results in an improved creep resistance. The copper-containing alloy

ACJMSX50 exhibits the highest resistance against compression creep. After the addition of 3 wt% zinc the minimum creep rate is comparable to that of alloy AJM50.

3.5 Corrosion in the Salt Spray Test

Fig. 11 displays the results of the salt spray tests for the copper-free alloys. Alloy AZ91D is included for comparison. Fig. 12 shows the corrosion rates of all alloys including AZ91D. Ground corrosion samples in general show a lower corrosion rate compared to as-cast samples. Addition of strontium, silicon and calcium hardly changes the corrosion resistance compared to the base alloy AM50. After the addition of 0.5 wt% copper, i.e., alloy ACJMSX50, a marked increase in the corrosion rate is observed. Alloying with 3 wt% zinc clearly has a positive effect on durability. However, the corrosion rates of as-cast and ground samples are still higher than 5 mm/y and considerably higher than those of AZ91D.

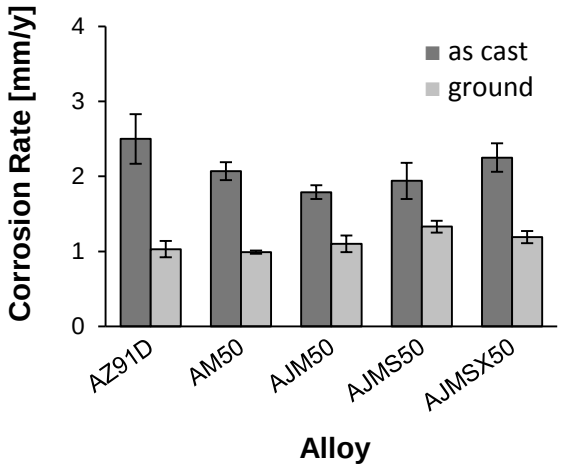

Fig. 11: Corrosion rates of Cu free alloys, 48 h salt spray test, 5 % NaCl, pH 7

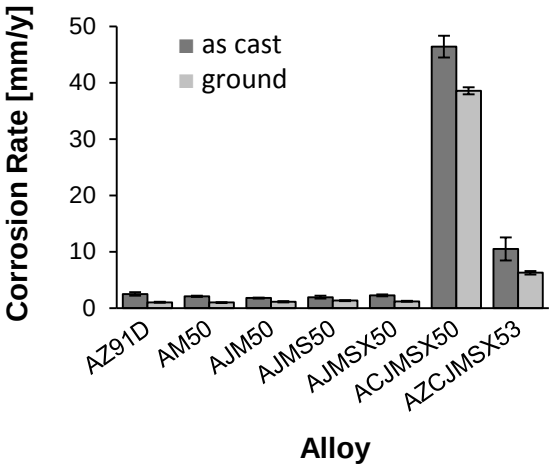

Fig. 12: Corrosion rates of all alloys, AZ91D included for comparison, 48 h salt spray test, 5 % NaCl, pH 7

4 Discussion

4.1 Phase Formation & Microstructure

The existence of phases in this article was proven by the XRD method. Results from EDX measurements were only used to locate phases in the microstructure and to gain information about the distribution of elements. Characteristic ratios of certain atom fractions strengthened the results from XRD measurements in some cases. However, with regard to the EDX measurements it has to be considered that precipitates in high pressure die cast magnesium alloys are small due to high cooling rates during solidification. The penetration depth of accelerated electrons increases with an increasing acceleration voltage of the scanning electron microscope and with a decreasing atomic number of the investigated material, see [31]. At an acceleration voltage of 15 kV, the influence of the magnesium matrix below an investigated precipitate becomes predominant in the interaction volume of the accelerated electrons. In this case, the magnesium content can be higher than expected from the elemental formula. In order to reduce the signal from the magnesium matrix, the acceleration voltage was sometimes set to 5 kV. The resultant measurements were always confirmed at acceleration voltages of 15 kV.

It is known from the literature that the α–matrix and the $Mg_{17}Al_{12}$ phase are the main constituents of the microstructure in the magnesium alloy AM50 [32]. The Al_4Sr, Mg_2Si and Al_2Ca phases have been reported as common precipitates in AJ, AS and AX alloys [19, 33, 34]. XRD investigations prove the formation of Al_4Sr after the addition of strontium. Strontium and silicon in alloy AJMS50 form the ternary Zintl phase $Sr_{6.33}Mg_{16.67}Si_{13}$. The elevated contents of oxygen and carbon detected by EDX measurements can be explained by a reaction of the precipitates in contact with

oxygen and carbon dioxide from air. A reaction from contact with the ingredients used for the metallographic preparation is also possible [25]. Both theses are supported by Nesper et al. [35]. They noted a decomposition of the $Sr_{6.33}Mg_{16.67}Si_{13}$ phase in contact with air and moisture. The $Sr_{6.33}Mg_{16.67}Si_{13}$ phase is detected in the microstructure even after the subsequent addition of calcium, copper and zinc as extra alloying elements. This finding is important for the recycling of mixed magnesium post-consumer scrap from ELVs.

The formation of the Al_4Sr phase could not be verified by XRD analysis in alloy ACJMSX50, but the presence of the phase is highly probable. A unique morphology of the Al-Sr precipitates was visible from the SEM pictures and the (Sr+Ca)/Al ratio of 3.7 is close to the stoichiometric ratio. As with the $Sr_{6.33}Mg_{16.67}Si_{13}$ phase, an exchange of strontium for calcium atoms in Al_4Sr is probable. Only one more aluminium-containing phase was found by EDX analysis, i.e. Mg-Al-Cu. The two peaks in the XRD pattern at 2θ of approximately 38° and 39° could only be assigned to the $Mg_{32}(Al,Zn)_{49}$ phase, also termed the τ-phase. However, the alloy contains almost no zinc. In the Al-Cu-Mg phase diagram, a phase exists which is very similar to $Mg_{32}(Al,Zn)_{49}$, i.e. $Mg_{32}(Al_x,Cu_{1-x})_{49}$, the T-phase [36]. Table 4 lists some crystallographic parameters of the two phases.

Table 4: Crystallographic characteristics of the $Mg_{32}(Al_x,Cu_{1-x})_{49}$ and $Mg_{32}(Al,Zn)_{49}$ phases [36]

Phase	Symbol	Pearson Symbol	Crystal Structure	Lattice parameter
$Mg_{32}(Al_x,Cu_{1-x})_{49}$	T	cI162	bcc	a=1428-1435
$Mg_{32}(Al,Zn)_{49}$	τ	cI162	bcc	a=1422

As can be seen, literature indicates an isomorphism of the τ- and the T-phase [36]. In 1935, Laves et al. reported isomorphism between a "$Mg_3Al_2Zn_3$" and a "Mg_4Al_6Cu"

phase [37]. It can therefore be assumed that the addition of copper to alloy AJMSX50 leads to the formation of $Mg_{32}(Al_x,Cu_{1-x})_{49}$. After the addition of zinc, EDX analysis revealed that $Mg_{32}(Al,Zn)_{49}$ precipitates in the AZCJMSX53 alloy dissolve copper, see Table 3. Neither pure $Mg_{32}(Al,Zn)_{49}$ nor pure $Mg_{32}(Al_x,Cu_{1-x})_{49}$ precipitates were found. Due to the similarities in the crystal structure, it seems probable that the two tau-phases can merge. Fig. 13 shows an isothermal cut of the Al-Mg-Zn phase diagram at room temperature calculated on the basis of thermodynamic data from Ohno et al. [38]. It can be seen that large variations in the Al/Zn ratio are possible. A mixture of the $Mg_{32}(Al_x,Cu_{1-x})_{49}$ and the $Mg_{32}(Al,Zn)_{49}$ phases would imply an exchange of Cu for Zn atoms. In this case the Al, Cu and Zn contents in the phase could vary to a large extent. This variation is what has been found by EDX analysis.

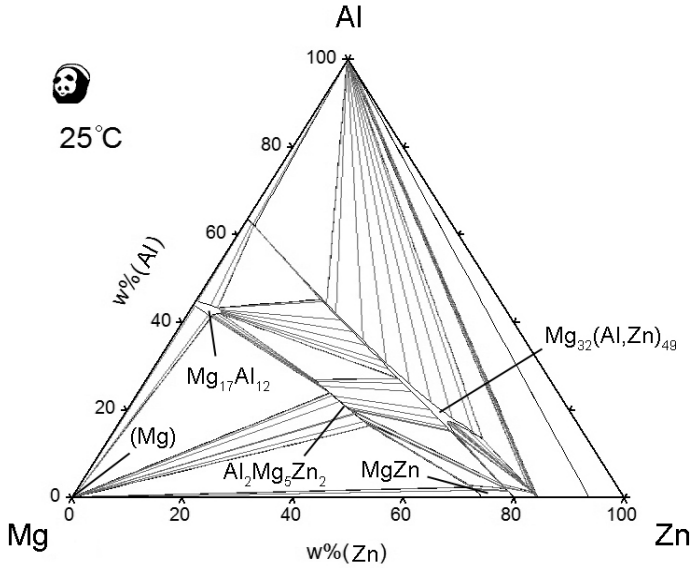

Fig. 13: Isothermal cut of Al-Mg-Zn phase diagram, room temperature, calculated from thermodynamic data according to [38]

4.2 Mechanical Properties in the Tensile Test

The specimen shape had a negative impact on the mechanical properties in the tensile test. According to ASTM standard B 94 - 07 [30], the HPDC base alloy AM50A should reach a yield strength of 110 MPa, an ultimate tensile strength of 200 MPa and an elongation at fracture of 10 %. These requirements are hardly fulfilled for the base alloy, especially with respect to the elongation at fracture, see Fig. 7. However, for tensile testing of HPDC magnesium alloys, specimens with a round cross-section and an undamaged casting skin are generally used [39, 40]. Berkmortel et al. [41] showed that round tensile specimens exhibited clearly improved mechanical properties compared to flat ones with a rectangular cross-section. Additionally, the casting skin of flat specimens machined for this project was missing on the cutting edges and, therefore, the yield strength was reduced. The level of porosity also affected the mechanical properties. The elongation at fracture and the ultimate tensile strength show contrarian developments compared to the level of porosity. The lowest porosity and the highest elongation at fracture were measured for alloy AJM50, whereas the highest porosity and the second-lowest elongation at fracture were measured for alloy AJMS50. The ultimate tensile strength and the elongation at fracture are linked as long as the specimen deforms in a uniform way. This was the case for all tensile specimens. Consequently, alloy AJM50 exhibited the highest and alloy AJMS50 the lowest ultimate tensile strength.

It has been shown that the grain diameter of castings can be reduced by increasing the content of certain alloying elements [42]. This phenomenon is known as solute grain refinement, and is described by the growth restriction factor (GRF). The principle of the GRF was established by Maxwell [43] for aluminium alloys and

adapted for magnesium alloys by StJohn et al. [44] and Lee et al. [42]. Amongst others, Lee et al. listed strontium, silicon, calcium, copper and zinc as elements with a grain refining effect. In this work, the process parameters such as melt and mould temperature were kept constant, and it can be assumed that the added alloying elements are responsible for the reduction of the grain size. The tensile yield strength increases because of the changes in the microstructure in accordance with the Hall-Petch equation. In the case of alloy AZCJMSX53, additional solid-solution strengthening of the α–matrix by means of zinc is probable. With regard to the remaining materials, only aluminium was detected in the matrix by EDX analysis [45].

The alloys AM50 and AZCJMSX53 showed comparable porosities but behaved differently in terms of the elongation at fracture. Based on the reduced grain diameters and the Hall-Petch equation, the zinc-containing material should have a higher ductility. In fact, alloy AZCJMSX53 exhibited the lowest elongation at fracture of the six materials. Westengen et al. [46] showed that the higher the content of the $Mg_{17}Al_{12}$ phase that forms upon alloying with aluminium, the lower the elongation at fracture. The $Mg_{17}Al_{12}$ phase is not present in alloy AZCJMSX53. Alloy ACJMSX50 exhibited an elongation at fracture nearly twice as high as for alloy AZCJMSX53. Therefore it is probable that the addition of zinc and the formation of the $Mg_{32}(Al,Zn)_{49}$ phase caused the reduction in ductility. The elongation at fracture of the secondary alloy AZCJMSX53 decreased by approximately 60 % compared to the base alloy AM50. However, it is more than twice as high compared to the secondary alloy AZC1232 [12].

4.3 Compression Creep Tests

Strontium, silicon and calcium are used to improve the creep resistance of commercial magnesium alloys. An elevated minimum creep rate has often been linked to an increased content of $Mg_{17}Al_{12}$ precipitates and the adjacent areas of the α-matrix being supersaturated with aluminium [33]. The formation of Al-containing intermetallics like Al_4Sr [19] and Al_2Ca [47] reduces the content of the $Mg_{17}Al_{12}$ phase and thereby improves creep resistance. The strengthening effect of silicon was attributed to the interaction of fine Mg_2Si particles and dislocations [48]. The creep resistance of the prepared alloys can be explained in the same way. After the addition of strontium to alloy AM50, aluminium is bound in the form of Al_4Sr and the creep rate decreases. When silicon is added to alloy AJM50, the ternary Zintl phase $Sr_{6.33}Mg_{16.67}Si_{13}$ forms, aluminium is released, and the creep rate increases again. Calcium in alloy AJMSX50 is partially solved in the $Sr_{6.33}Mg_{16.67}Si_{13}$ phase and replaces strontium but also forms aluminium-containing precipitates. The replacement of strontium is shown by the elevated XRD peaks of the Al_4Sr phase, see Fig. 1, and the formation of Al-Ca-precipitates was found by EDX analysis in alloy AJMSX50 [22]. Because the two alloying elements bind aluminium, the creep rate decreases. Copper, according to results from EDX and XRD investigations, completely suppressed the formation of the $Mg_{17}Al_{12}$ phase. The creep rate reached the lowest value of all the alloys prepared by HPDC in this study. The $Mg_{32}(Al,Zn)_{49}$ phase formed after the addition of zinc, and the creep rate increased again. According to the XRD patterns in Fig. 2, the content of $Mg_{17}Al_{12}$ remains unchanged when comparing the alloys ACJMSX50 and AZCJMSX53. Because no negative impact on the creep rate was found for the $Sr_{6.33}Mg_{16.67}Si_{13}$ phase [25], it seems probable that the $Mg_{32}(Al,Zn)_{49}$ phase has a limited thermal stability.

4.4 Corrosion in the Salt Spray Test

The detrimental effect of copper on the corrosion properties of magnesium alloys is well known [49]. Only a small number of phases have been identified by XRD in the microstructure after the addition of copper. $Sr_{6.33}Mg_{16.67}Si_{13}$ precipitates in alloy ACJMSX50 contain only little if any copper. Al-Sr precipitates do contain 4.5 % copper. However, the content is not high enough to cause observable peaks in the XRD graph. Therefore, due to the higher volume fraction and the higher copper concentration it is assumed that the $Mg_{32}(Al_x,Cu_{1-x})_{49}$ phase caused the increased corrosion rate. After the addition of zinc, Al-Sr precipitates were not found even by EDX measurements and the only copper-containing phase is the τ-phase $Mg_{32}(Al,Zn)_{49}$. Accordingly, the improved corrosion resistance of alloy AZCJMSX53 compared to alloy ACJMSX50 is ascribed to the formation of the τ-phase $Mg_{32}(Al,Zn)_{49}$. The zinc-containing precipitates have a much lower impact on the materials corrosion rate compared to precipitates of the Al-Sr and the $Mg_{32}(Al_x,Cu_{1-x})_{49}$ phase. Lunder et al. [50] stated that precipitates with a high electrochemical potential are likely to cause galvanic corrosion in contact with the α-matrix. Blawert et al. [11] investigated the $Mg_{32}(Al,Zn)_{49}$ phase and its influence on the corrosion of magnesium in detail. They found that the $Mg_{32}(Al,Zn)_{49}$ phase is even more noble than the $Mg_{32}(Al_x,Cu_{1-x})_{49}$ phase when compared to the magnesium matrix. According to Blawert et al. [11] the improved corrosion properties after zinc addition are in fact caused by an elevated hydrogen overvoltage of the $Mg_{32}(Al,Zn)_{49}$ phase in connection to the α-matrix. It is important to remember that the $Sr_{6.33}Mg_{16.67}Si_{13}$ phase does not solve aluminium. Because the ternary Zintl phase can incorporate strontium and calcium, the formation of aluminium-containing phases, such as Al_4Sr,

$Mg_{17}Sr_2$, Al_2Ca and or Al_4Ca, is prevented as long as the correct ratio of strontium, silicon and calcium is maintained. The Sr/Si ratio of mass-fractions in the $Sr_{6.33}Mg_{16.67}Si_{13}$ phase is 1.52. If this ratio is adjusted in the alloy, the maximum aluminium content is available for the formation of the $Mg_{32}(Al,Zn)_{49}$ phase. So far, no negative influence of the $Sr_{6.33}Mg_{16.67}Si_{13}$ phase on the corrosion properties of AM-based magnesium alloys has been found [23]. One reason might be the characteristics of Zintl phases. Gottstein [51] reported a high stoichiometry and predominantly polar bonding. According to Lunder et al. [50] the binary Zintl phase Mg_2Si is one of the few intermetallic phases which is not detrimental to the corrosion properties of magnesium alloys.

Further improvements in the corrosion resistance may be possible with variations in the zinc, copper and aluminium contents within the $Mg_{32}(Al,Zn)_{49}$ phase. The issue of nickel contamination was not addressed in the present work, but according to Hanawalt et al. [49] the addition of zinc to magnesium-aluminium-manganese alloys also had a positive influence in this respect.

5 Conclusions

Six magnesium alloys were prepared by HPDC in order to develop a secondary alloy for mixed post-consumer scrap from ELVs. Moderate additions of strontium, silicon and calcium represented the input of alloying elements from cost-competitive, heat-resistant alloys due to intermixing during the shredder process. Copper was added to consider the effect of impurities. The addition of zinc proved to be capable of compensating for the previous contamination. The results of the investigations can be summarised as follows:

1. The ternary Zintl phase $Sr_{6.33}Mg_{16.67}Si_{13}$ forms in alloy AM50 after the addition of strontium and silicon. The phase is stable even in the presence of calcium, copper and zinc.

2. Upon the addition of 0.5 % copper, the formation of the $Mg_{32}(Al_x,Cu_{1-x})_{49}$ phase in alloy ACJMSX50 was observed. The corrosion resistance of the alloy in the salt spray test markedly decreased, whilst the resistance to compression creep increased.

3. The addition of 3.0 % zinc to alloy ACJMSX50 resulted in the formation of the tau-phase $Mg_{32}(Al,Zn)_{49}$. The detrimental effect of copper on the corrosion resistance was clearly reduced.

4. Isomorphism reported in literature as well as the results from XRD and EDX measurements strongly suggest that the $Mg_{32}(Al_x,Cu_{1-x})_{49}$ and the $Mg_{32}(Al,Zn)_{49}$ phases can merge. According to thermodynamic calculations, the phase transition implies large variations in the zinc, copper and aluminium contents within the precipitates. This finding is supported by experimental results.

5. The subsequent addition of strontium, silicon, calcium, copper and zinc reduced the grain size of the prepared alloys. This effect was probably caused by the solute grain refinement and had a positive influence on the yield strength of the materials.

The formation and coexistence of the ternary Zintl phase $Sr_{6.33}Mg_{16.67}Si_{13}$ and the tau-phase $Mg_{32}(Al,Zn)_{49}$ in one alloy offers the most attractive system for magnesium recycling from post-consumer scrap containing strontium, silicon and calcium. The Zintl phase has a limited impact on the material properties. Copper as an impurity is

incorporated into the tau-phase, and its detrimental effect is thereby considerably reduced. As long as strontium, silicon and calcium are in the right proportions, the formation of aluminium-containing strontium or calcium phases is prevented, and the entire aluminium content is available for the formation of the $Mg_{32}(Al,Zn)_{49}$ phase.

In order to develop a secondary alloy with reasonable ductility, an aluminium content of 5 wt% and a zinc content of 3 wt% proved to be useful, see [11]. The addition of 1.1 wt% strontium, silicon and calcium reduced the elongation at fracture by approximately 20 %. The contents of the latter three alloying elements represent guide values. Calcium is not necessary to form the ternary Zintl phase $Sr_{6.33}Mg_{16.67}Si_{13}$. At any rate, the Sr/Si ratio of 1.52 can be used to avoid the formation of aluminium-strontium phases. The content of strontium, silicon and calcium in emerging scrap fractions from ELVs cannot be foreseen, but alloying elements, when lacking, can be added to achieve the desired composition.

The concept of a secondary magnesium alloy presented in this paper demonstrates that it is possible to manage the problems of mixed alloying elements and contamination with impurities in one alloy system. The present work promotes the idea of recycling magnesium components from ELVs by re-melting and thus using minimal primary materials and energy.

Acknowledgements

The authors want to thank Professor Schmid-Fetzer from the Technische Universität Clausthal for the calculation of the isothermal cut of the Al-Mg-Zn system. This work

was supported by the Deutsche Forschungsgemeinschaft within the program 1168 “InnoMagTec”.

References

[1] U. S. Department of Interior, U. S. Geological Survey, Mineral Commodity Summaries 2009, Magnesium Metal, (2009), http://minerals.usgs.gov/minerals/pubs/mcs/2009/mcs2009.pdf.
[2] U. S. Department of Interior, U. S. Geological Survey, Mineral Commodity Summaries 2003, Magnesium Metal, (2003), http://minerals.usgs.gov/minerals/pubs/mcs/2003/mcs2003.pdf.
[3] U. S. Department of Interior, U. S. Geological Survey, Mineral Commodity Summaries 1996, Magnesium Metal, (1996), http://minerals.usgs.gov/minerals/pubs/commodity/magnesium/mgmetmcs96.pdf.
[4] A.J. Gesing, A. Dubreuil: Recycling of Post-Consumer Mg Scrap, in, 65th Annual World Magnesium Conference, Warsaw, PL, International Magnesium Association, (2008), pp. 131-142.
[5] C. Scharf, C. Blawert, A. Ditze: Application of Remelted Post Consumer Scrap for Structural Magnesium Parts, in: K.U. Kainer (Ed.), Magnesium Alloys and Their Applications, Wolfsburg, D, Wiley-VCH, (2003), pp. 980-987.
[6] A. Ditze, C. Scharf, Recycling of Magnesium, 1 ed., Papierflieger Verlag, 2008.
[7] A. Tharumarajah, P. Koltun: Lifecycle Assessment of Magnesium Component Supply Chain, in, 62nd Annual World Magnesium Conference, Berlin, D, International Magnesium Association, (2005), pp. [8].
[8] G. Franke: Industrial Recycling of Magnesium Alloys, in: W. Ding (Ed.), Sinomag Die Casting Magnesium Seminar, Beijing, PRC, private publisher, (2000), pp. 237-245.
[9] T.B. Zhu, N.Y. Li, X.M. Mei, A. Yu, S.X. Shang: Innovative Vacuum Distillation for Magnesium Recycling, in: J.N. Hryn (Ed.), TMS Annual Meeting, New Orleans, USA, Minerals, Metals & Materials Soc, (2001), pp. 55-60.
[10] I.A. Barannik, V.N. Devyatkin: Structure of Magnesium Alloys Usage in USSR. Secondary Metal Processing, in: B.L. Mordike, F. Hehmann (Eds.), Magnesium Alloys and Their Applications, Garmisch-Partenkirchen, D, DGM Informationsgesellschaft, Oberursel, Germany, (1997), pp. 43-49.
[11] C. Blawert, D. Fechner, D. Höche, V. Heitmann, W. Dietzel, K.U. Kainer, P. Zivanovic, C. Scharf, A. Ditze, J. Gröbner, R. Schmid-Fetzer, Corrosion Sci., 52 (2010) 2452–2468.
[12] C. Blawert, E. Morales, K.U. Kainer, C. Scharf, P. Živanović, A. Ditze: Development of a New AZ Based Secondary Magnesium Alloy, in, 65th Annual World Magnesium Conference, Warsaw, PL, International Magnesium Association, (2008), pp. [8].
[13] C. Scharf, P. Zivanovic, A. Ditze, D. Fechner, C. Blawert, K.U. Kainer: Corrosion Resistant Magnesium Recycling Alloys, in: K.U. Kainer (Ed.), Magnesium - 8th International Conference on Magnesium Alloys and their Applications, Weimar, Germany, Wiley-VCH, (2009), pp. 1308-1315.

[14] Patent No.: WO 2007009435-A1 (13.07.2006), A. Ditze, C. Scharf, C. Blawert, K.U. Kainer, E.D. Morales Garza, Technische Universität Clausthal, D, GKSS-Forschungszentrum Geesthacht GmbH, D
[15] Patent No.: EP 2 116 622 A1 (21.04.2009), C. Blawert, K.U. Kainer, W. Dietzel, A. Ditze, C. Scharf, P. Zivanovic, GKSS-Forschungszentrum Geesthacht GmbH.
[16] Magnesium Technology, Hrsg.: H.E. Friedrich, B.L. Mordike, Springer Verlag, 2006.
[17] A. Barth: Mg-Application in the 7G-Tronic-Gear, in, 61st Annual World Magnesium Conference, New Orleans, USA, International Magnesium Association, (2004), pp. [14].
[18] J. Wolf, W. Wagener: The BMW Magnesium-Aluminium Crankcase, a Challenge for State-of-the-Art Light Metal Casting, in, 62nd Annual World Magnesium Conference, Berlin, D, International Magnesium Association, (2005), pp. [8].
[19] M.O. Pekguleryuz, E. Baril: Development of Creep Resistant Mg-Al-Sr Alloys, in: J.N. Hryn (Ed.), TMS Annual Meeting, New Orleans, USA, Minerals, Metals & Materials Soc, (2001), pp. 119-125.
[20] Patent No.: US 6139651-A (04.08.1999), B. Bronfin, E. Aghion, S. Schuhmann, P. Bohling, K.U. Kainer, Dead Sea Magnesium, IL; Volkswagen AG, D.
[21] J.R. TerBush, J.W. Jones, T.M. Pollock: A Comparative Examination of Aging and Creep Behavior of Die-Cast MRI230D and AXJ530, in: M.O. Pekguleryuz, N.R. Neelameggham, R.S. Beals, E.A. Nyberg (Eds.), TMS Annual Meeting, New Orleans, USA, Minerals, Metals & Materials Soc, (2008), pp. 117-122.
[22] D. Fechner, N. Hort, K.U. Kainer: Magnesium Recycling System Prepared by Permanent Mould- and High Pressure Die Casting, in: E.A. Nyberg, S.R. Agnew, M.R. Neelameggham, M.O. Pekguleryuz (Eds.), TMS Annual Meeting, San Francisco, USA, Minerals, Metals & Materials Soc, (2009), pp. 111-116.
[23] D. Fechner, C. Blawert, N. Hort, K.U. Kainer: Influence of Strontium, Silicon and Calcium Additions on the Properties of the AM50 Alloy, in: M.S. Dargusch, S.M. Keay (Eds.), Light Metals Technology 2009, Gold Coast, Queensland, Australia, Trans Tech Publications Ltd., (2009), pp. 459-462.
[24] D. Fechner, C. Blawert, N. Hort, K.U. Kainer, Sci. China Ser. E-Technol. Sci., 52 (2009) 148-154.
[25] D. Fechner, N. Hort, C. Blawert, H. Dieringa, M. Störmer, K.U. Kainer, J. Mater. Sci., 47 (2012) 5461-5469.
[26] ASTM E 112 - 96, Standard Test Methods for Determining Average Grain Size, (1996).
[27] DIN 10002-1, Metallische Werkstoffe Zugversuch, (2001).
[28] DIN 50125, Prüfung Metallischer Werkstoffe - Zugproben, (2004).
[29] ASTM B 117 - 07, Standard Practice for Operating Salt Spray (Fog) Apparatus, (2007).
[30] ASTM B 94 - 07, Standard Specification for Magnesium-Alloy Die Castings, (2007).
[31] P.F. Schmidt, L.J. Balk, R. Blaschke, E. Demm, L. Engel, R. Göcke, H. Hantsche, R. Hauert, E.R. Krefting, T. Müller, H. Raith, M. Roth, J. Wootdthli, Praxis der Rasterelektronenmikroskopie und der Mikrobereichsalanyse, expert Verlag, 1994.
[32] P. Zhao, Q.D. Wang, C.Q. Zhai, Y.P. Zhu, Materials Science and Engineering A, 444 (2007) 318-326.
[33] M.S. Dargusch, G.L. Dunlop, K. Pettersen: Elevated Temperature Creep and Microstructure of Die Cast Mg-Al Alloys, in: B.L. Mordike, K.U. Kainer (Eds.),

Magnesium Alloys and Their Applications, Wolfsburg, D, Werkstoff-Informationsgesellschaft mbH, (1998), pp. 277-282.
[34] K.Y. Sohn, J.W. Jones, J.E. Allison: The Effect of Calcium on Creep and Bolt Load Retention Behavior of Die-Cast AM50 Alloy, in: H.L. Kaplan, J.N. Hryn, B.B. Clow (Eds.), TMS Annual Meeting, Nashville, USA, Minerals, Metals & Materials Soc, (2000), pp. 271-278.
[35] R. Nesper, S. Wengert, F. Zurcher, A. Currao, Chem.-Eur. J., 5 (1999) 3382-3389.
[36] Ternary Alloys, Hrsg.: G. Petzow, G. Effenberg, VCH Verlagsgesellschaft, 1993.
[37] F. Laves, K. Löhberg, H. Witte, Metall-Wirtschaft, -Wissenschaft und -Technik, 14 (1935) 793-794.
[38] M. Ohno, D. Mirkovic, R. Schmid-Fetzer, Mater. Sci. Eng. A-Struct. Mater. Prop. Microstruct. Process., 421 (2006) 328-337.
[39] P. Labelle, M. Pekguleryuz, D. Argo, M. Dierks, T. Sparks, T. Waltematte, in: SAE World Congress, Detroit, USA, 2001, pp. [8].
[40] ASTM B 557M - 06, Standard Test Methods for Tension Testing Wrought and Cast Aluminium- and Magnesium-Alloy Products [Metric], (2006).
[41] R. Berkmortel, G.G. Wang, P. Bakke: Fluxless In-House Recycling of High Purity Magnesium Die Cast Alloys at Meridian Operations, in, 57th Annual World Magnesium Conference, Vancouver, CDN, International Magnesium Association, (2000), pp. 22-27.
[42] Y.C. Lee, A.K. Dahle, D.H. StJohn, Metallurgical and Materials Transactions A, 31 (2000) 2895-2906.
[43] I. Maxwell, A. Hellawell, Acta Metallurgica, 23 (1975) 229-237.
[44] D.H. StJohn, M. Qian, M.A. Easton, P. Cao, Z. Hildebrand, Metallurgical and Materials Transactions A, 36 (2005) 1669-1679.
[45] D. Fechner: Entwicklung einer Magnesium-Recyclinglegierung auf Basis der Legierung AM50, Dr., Technische Universtität Clausthal, Clausthal, Germany, (2010), S. 161.
[46] H. Westengen, T.K. Aune, Casting Alloys, in: H.E. Friedrich, B.L. Mordike (Eds.) Magnesium Technology, Springer Verlag, 2006, pp. 145-204.
[47] K.Y. Sohn, J.W. Jones, J. Berkmortel, H. Hu, J.E. Allison, in: SAE World Congress, Detroit, USA, 2000, pp. 1-9.
[48] E. Evangelista, S. Spigarelli, M. Cabibbo, C. Scalabroni, O. Lohne, P. Ulseth, Mater. Sci. Eng. A-Struct. Mater. Prop. Microstruct. Process., 410 (2005) 62-66.
[49] C.E.N. J. D. Hanawalt, J. A. Peloubet, Transactions of the American Institute of Mining and Metallurgical Engineers, 147 (1942) 273-299.
[50] O. Lunder, K. Nisancioglu, R.S. Hansen, in: International Congress and Exposition, Detroit, USA, 1993, pp. 117-126.
[51] G. Gottstein, Physikalische Grundlagen der Materialkunde, 3 ed., Springer Verlag, 2007.